Understanding the Insulating Phase in Colossal Magnetoresistance Manganites: Shortening of the Jahn-Teller Long-Bond across the Phase Diagram of $La_{1-x}Ca_xMnO_3$

E. S. Božin,[1] M. Schmidt,[2] A. J. DeConinck,[1] G. Paglia,[1] J. F. Mitchell,[3] T. Chatterji,[4] P. G. Radaelli,[2] Th. Proffen,[5] and S. J. L. Billinge[1]

[1]*Department of Physics and Astronomy, Michigan State University, East Lansing, Michigan 48824-2320, USA*
[2]*ISIS, CCLRC Rutherford Appleton Laboratory, Chilton-Didcot, OX11 0QX, Oxfordshire, United Kingdom*
[3]*Materials Science Division, Argonne National Laboratory, Argonne, Illinois 60439, USA*
[4]*Institute Laue-Langevin, Boîte Postale 156, 38042 Grenoble Cedex 9, France*
[5]*Lujan Neutron Scattering Center, Los Alamos National Laboratory, Los Alamos, New Mexico 87545, USA*

(Received 19 September 2006; published 27 March 2007)

The detailed evolution of the magnitude of the local Jahn-Teller (JT) distortion in $La_{1-x}Ca_xMnO_3$ is obtained across the phase diagram for $0 \leq x \leq 0.5$ from high-quality neutron diffraction data using the atomic pair distribution function method. A local JT distortion is observed in the insulating phase for all Ca concentrations studied. However, in contrast with earlier local structure studies, its magnitude is not constant, but *decreases* continuously with increasing Ca content. This observation is at odds with a simple small-polaron picture for the insulating state.

DOI: 10.1103/PhysRevLett.98.137203 PACS numbers: 75.47.Gk, 61.12.−q, 71.38.−k, 75.47.Lx

Doped transition metal oxides are of fundamental interest for their electronic properties that exhibit various types of colossal responses such as high-temperature superconductivity, colossal magnetoresistance (CMR), and ferroelectricity [1], which are still not fully understood. A recent concept that may be relevant for many of these systems is the observation of nanoscale inhomogeneities that are thought to be intrinsic. These can take the form of nanoscale checkerboard [2,3] or stripe patterns [4], or less ordered structures [5–8] that are related to electronic phase separation. Phase separation is also found theoretically in computational models, which have been used to explain the large changes in conductivity with temperature and doping [9]. However, the ubiquity and fundamental importance of electronic inhomogeneities to the colossal effects is not completely established [10]. For example, local-probe experiments where no electronic inhomogeneities are observed have been made on samples that show a colossal response [11,12] and some observed inhomogeneities have been related to disorder in the chemical dopant ions [13].

One approach for establishing a correlation between inhomogeneities and electronic properties is to study the complete phase diagram of interesting systems. We set out to examine the local structure of the $La_{1-x}Ca_xMnO_3$ (LCMO) manganite family. This is an archetypal system for such studies because of the strong electron-phonon coupling, through the JT effect, resulting in a large structural response to electronic phase separation. We probe this using the atomic pair distribution function (PDF) measured from neutron powder diffraction data. The signature of the metallic phase in local structural probes is the absence of a JT-long-bond [14,15]. When the charges are localized in a polaronic insulating phase, the JT-long-bond is seen [14–18]. A two phase fit of an undistorted and distorted phase to the low-r region of the PDF can thus yield a quantitative measure of the phase fraction of each phase as a function of T and x in the system $La_{1-x}Ca_xMnO_3$ [19]. Unexpectedly, we found that the *length* of the Jahn-Teller long-bond in the insulating phase decreases continuously with increasing doping in this system, contrary to the canonical understanding [17,18,20,21]. Here we report for the first time extensive, high real-space resolution PDF data as a function of temperature and doping from $0 \leq x \leq 0.5$ on well characterized samples in the $La_{1-x}Ca_xMnO_3$ system using new high-resolution, high-throughput, time-of-flight neutron diffractometers. We rule out the existence of fully JT distorted long-bonds at 2.16 Å in the CMR compositions that would be expected in a simple single-site small-polaron scenario for the phase above T_c. The smooth continuous decrease in the length of the JT-long-bond is most easily explained in a delocalized or large polaron picture.

A series of 13 powdered LCMO samples with compositions spanning $0 \leq x \leq 0.5$ range were prepared using standard solid state synthesis methods and annealed to ensure oxygen stoichiometry [22] and characterized by resistivity and magnetization measurements. Two additional finely pulverized single crystal samples ($x = 0.075$, 0.1), grown by the floating zone method utilizing image furnace, were also used to increase coverage of the phase space under the study. Neutron powder diffraction measurements were carried out at the GEM diffractometer at the ISIS facility at the Rutherford Appleton Laboratory in the UK and at the NPDF diffractometer at Los Alamos Neutron Scattering Center. The samples, of approximately 6 grams each, were loaded into extruded vanadium containers and sealed under He atmosphere. The data were collected for all the samples at a consistent set of 7 temperatures between 10 K and 550 K using a closed cycle He refrigerator. The data were processed to obtain PDFs [23] using the program PDFGETN [24] by a sine Fourier trans-

form of the total scattering structure function $F(Q)$ up to a value of Q_{max} of 35 Å^{-1}. This high Q_{max}, coupled with the good statistics from GEM and NPDF, result in high-quality PDFs with minimal spurious low-r ripples and negligible termination ripples, as evident in Fig. 1. The PDF analysis reported here involves both direct data evaluation and structural modeling using the program PDFFIT [25]. Results of complementary average crystal structure modeling, carried out using the program GSAS [26], are also presented. All refinements were carried out using the O or O' structural models in the $Pbnm$ space group with isotropic displacement parameters [27]. Our analysis does not address the ordering of localized charges such as observed in the charge ordered state at $x = 0.5$ [28].

The results of the average crystal structure evaluation is summarized in Figs. 2(a) and 3. In the orthorhombic O phase [29], the *local* JT distortion amplitude (the length of the JT-long-bond) is the same as the average long range ordered value. The distortion is constant with temperature for fixed Ca content, but decreases linearly with increasing Ca content. Upon crossing into the pseudocubic O' phase, the average JT distortion disappears abruptly [Fig. 2(a) and 3]. However, this effect is accompanied by the anomalous increase of the isotropic thermal parameters on oxygen sites, Fig. 2(d). This is consistent with the understanding that the pseudocubic O' phase in the insulating state consists of orbitally disordered, JT distorted, octahedra [30,31], and that this picture can be extended to finite doping. In the ferromagnetic metallic (FM) phase, the Rietveld refined JT-long-bond disappears, but there is no significant enlargement of the refined oxygen thermal parameter showing that the local JT-long-bond is also absent [14]. Structural refinements to the PDF data over a wide range of r ($r_{max} = 20$ Å) mimic the Rietveld results rather closely [Fig. 2(b) and 2(e)]. This shows that the average structure result is already obtained for a PDF refinement over a 20 Å range, suggesting that the size of local orbital ordering correlations is limited to this range.

The size and shape of the local MnO_6 octahedra can be obtained by fitting the PDF over a narrow r range of 6 Å. The length of the local long Mn-O bond has been obtained

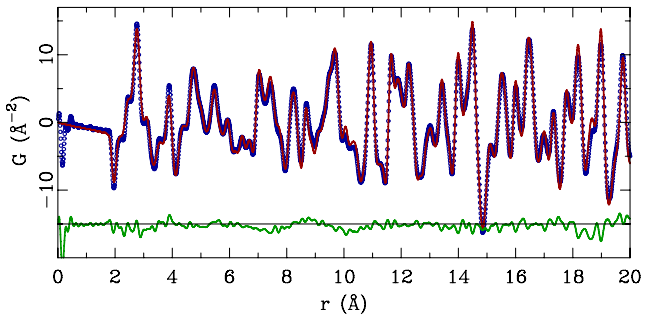

FIG. 1 (color online). ○ are the $G(r)$ of $x = 0.22$ sample at 10 K; solid red line is the calculated $G(r)$ from the crystal structure model. The difference curve is shown offset below.

for all compositions and temperatures studied, and is shown as a contour plot in Fig. 2(c). The color scale has been set such that a fully shortened long-bond of 1.96 Å shows up as black. The presence of color therefore indicates a finite local JT distortion. There is a striking resemblance between the contour plot of the local JT-long-bond in Fig. 2(c) and the electronic phase diagram of this manganite that is superimposed. The position of the phase transition lines were verified from magnetization and resistivity measurements of the samples used in this study.

First, we note that the *local* JT distortion is present in the entire insulating part of the phase diagram, but that it is effectively removed for the metallic compositions at lowest temperatures. Second, it is seen that the *magnitude* of the local JT distortion has a relatively strong doping dependence at lower Ca concentrations, with the bond length versus concentration curve flattening at higher Ca doping levels.

Selected constant temperature cuts are shown in Fig. 3(a)–3(c), for 550 K, 250 K, and 10 K, respectively. The square symbols show the behavior of the average structure. The JT-long-bond decreases with doping in the orbitally ordered O phase, but then abruptly shortens at the structural phase transition, indicated by the dotted line in the figure. In contrast, the local JT bond is insensitive to the

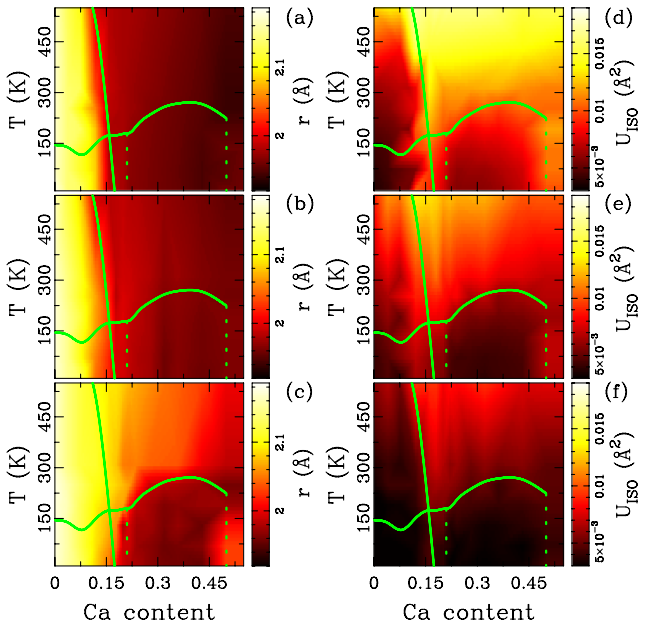

FIG. 2 (color online). Contour plot of the JT distortion (long Mn-O distance) in (x, T) parameter space as obtained from (a) Rietveld analysis and PDF analyses over (b) 20 Å and (c) 6 Å ranges, respectively. Contour plot of the isotropic displacement parameter of oxygen, $U_{iso}(O2)$ in $Pbnm$ setting, as obtained from (d) Rietveld analysis, and PDF analyses over (e) 20 Å and (f) 6 Å ranges. In all the panels the solid curves indicate T_{JT} and T_c phase lines, while dotted vertical lines indicate IM phase boundaries, as determined from the sample characterization measurements.

structural transition, but disappears abruptly when the sample goes through the insulator-metal (IM) transition. This is consistent with the widely held current view [14,15]. What is less expected is the observation that the *length* of the local JT-long-bond shortens with increasing doping in the insulating state. In a single-site small-polaron picture the insulating state consists of distinct Mn^{3+} and Mn^{4+} sites. The 4+ sites are presumed to have regular, undistorted, MnO_6 octahedra and the 3+ sites to be JT distorted with 2.16 Å long bonds, as in the undoped $LaMnO_3$ end member, and this was supported by experimental evidence [15,17,18]. We investigate these refinement results in greater detail below.

Figure 4 shows some representative PDF data bracketing the IM transition. We show the nearest-neighbor doublet of the PDF from $La_{1-x}Ca_xMnO_3$ with $x = 0.18$ and $x = 0.22$. The former sample remains in the insulating state at all temperatures; the latter is a ferromagnetic metal below ~180 K, and paramagnetic insulator at higher temperature. Thus, a comparison of the curves in Fig. 4(b) shows the effect of changing composition without crossing the IM transition. The changes are very small. In Fig. 4(a) the metal insulator (MI) is crossed at constant temperature. The changes to the nearest-neighbor doublet on crossing the MI transition are evident with a sharp, single-valued peak giving way to a peak with a well-defined shoulder on the high-r side. This is the appearance of the JT-long-bond in the insulating phase. Notable, however, is the absence of intensity at the position of the undoped JT-long-bond at $r = 2.16$ Å, indicated by a vertical dashed line in the figure. This clearly shows the absence of any fully distorted JT octahedra in the structure. The difference curve in Fig. 4(a) also shows the appearance of intensity on the low-r side of the shortest bond in the insulating phase. Figure 4(c) and 4(d) shows the model fits to the metallic and insulating PDFs, giving a sense of the quality of fits to the local PDF that were obtained in our determination of the phase diagram in Figs. 2 and 3.

The main result of the current study is the clear demonstration of an absence of any Mn-O long-bonds of the fully JT distorted 2.16 Å length in the doped samples, as would be expected in a simple-minded small-polaron picture. Our result disagrees with the canonical understanding from earlier experimental studies [15,17,18], though is consistent with the observations of a number of less well-known studies [32,33]. The observation could be explained in a homogeneous picture where the electron density is uniformly distributed over all Mn sites in the insulating state. In this case, the electron density in the orbitals, and therefore the driving force for the JT distortion, decreases continuously with increasing hole doping. It is harder to explain in a small-polaron picture where localized Mn^{4+} sites exist in a fully distorted Mn^{3+} background. In this scenario, one source of long-bond shortening could be elastic strain in the lattice because of the disordered polarons. This is unlikely to explain our observation. The energy scale for octahedral rotations is much smaller than for stretching the covalent bonds [34] and most elastic strain accommodation is expected to occur in the octahedral rotations. This is indeed the case when orbital disorder sets in at constant doping as a function of temperature [30]. Also, we note that there is a negative deviation from Vegard's law [35], indicated by the dashed line in Fig. 3, in the average length of the long-bond. Elastic

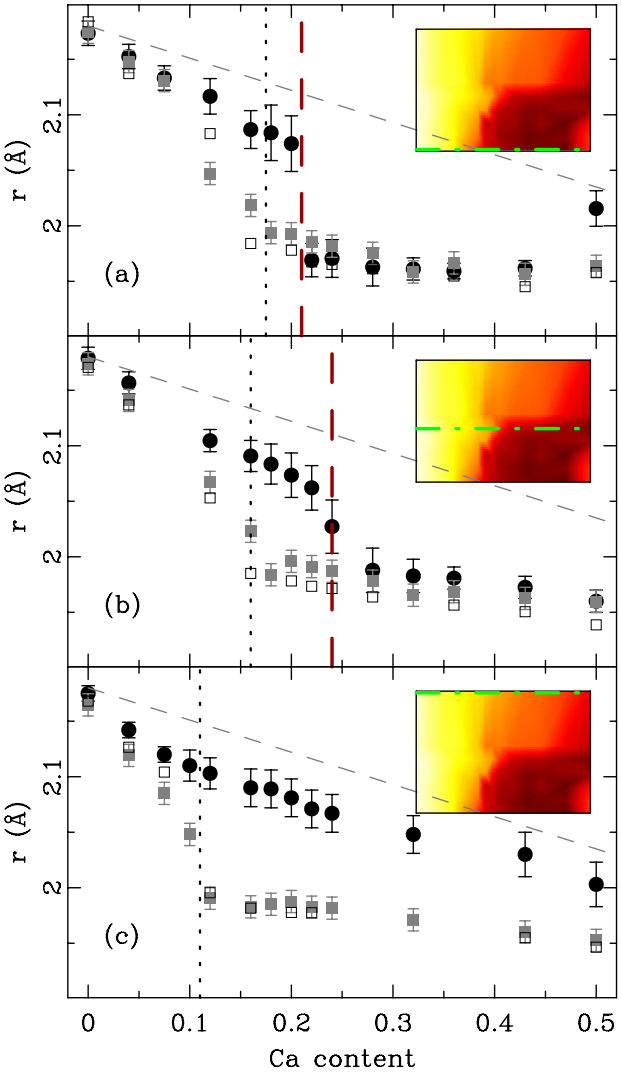

FIG. 3 (color online). Length of the longest Mn-O distance in the MnO_6 octahedron vs doping at (a) 10 K, (b) 250 K, and (c) 550 K. □ denote Rietveld result; ■ and ● show results of PDF refinements over 20 Å and 6 Å ranges, respectively. Sloping dashed lines denote Vegard's law [35] behavior for Mn-O long-bond interpolating between the values for $LaMnO_3$ and $CaMnO_3$. Dashed vertical lines mark the IM transition, while the dotted vertical lines denote the orthorhombic to pseudocubic phase transition. The insets reproduce Fig. 2(c) showing the temperature of the data shown in the panel. Symbols indicate measured compositions.

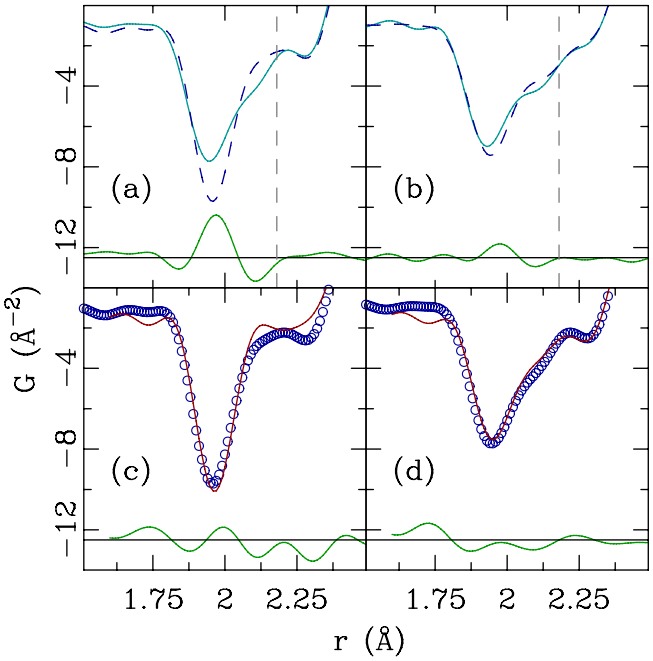

FIG. 4 (color online). Experimental PDFs, $G(r)$, of $x = 0.18$ (solid line) and $x = 0.22$ (dashed line) samples at (a) 10 K and (b) 190 K, with difference curves underneath. Both data sets are in the insulating phase in (b) but straddle the IM boundary in (a). A JT long-bond appears in the insulating phase but is shorter than that in the undoped end member, indicated by the vertical dashed lines. (c) and (d) show representative $r_{\max} = 6$ Å PDF fits (solid lines) to the 10 K data (○) shown in (a). Difference curves are offset below.

relaxation in covalently bonded alloys analogous to the manganites results in a characteristic Z plot [36,37] of bond-length versus composition that is clearly not seen here. A principle strain relaxation mode through octahedral rotations is also indicated by enlarged U_{iso} values in the insulating region of the phase diagram, as evident in Fig. 2(d). We also note that oxygen K edge spectroscopy indicates an increasing importance of oxygen ligand hole states with doping [38,39], indicating a clear change in the local electronic structure induced by doping.

It is not possible from our current data to tell unambiguously whether or not the sample is phase separated into metallic and insulating regions. Phase separation would imply a transfer of intensity from the position of the long-bond to that of the short-bond. What we show here is that the length of the long-bond decreases with doping. The long-bond starts to overlap with the short-bond at higher doping making an extraction of the integrated area of the peak uncertain. However, we note that modeling the local structure with a homogeneous model in *Pbnm* setting as we have done, with 4 short and 2 long-bonds at all doping levels in the insulating region, results in rather good fits as evident in Figs. 1 and 4(d). Enlarged oxygen U_{iso} values in $0.12 \leq x \leq 0.17$ range are evident in Fig. 2(d)–2(f) where phase separation has been observed [40].

We acknowledge discussions with S. D. Mahanti, P. M. Duxbury, T. A. Kaplan, and P. Juhás. Work at MSU was supported by the NSF under Grant No. DMR-0304391, Argonne by DOE under Contract No. DE-AC02-06CH11375, and Los Alamos under Contract No. DE-AC52-06NA25396.

[1] A. J. Millis, Nature (London) **392**, 147 (1998).
[2] S. Komiya *et al.*, Phys. Rev. Lett. **94**, 207004 (2005).
[3] T. Hanaguri *et al.*, Nature (London) **430**, 1001 (2004).
[4] J. M. Tranquada *et al.*, Nature (London) **375**, 561 (1995).
[5] M. Fath *et al.*, Science **285**, 1540 (1999).
[6] M. Uehara *et al.*, Nature (London) **399**, 560 (1999).
[7] T. Becker *et al.*, Phys. Rev. Lett. **89**, 237203 (2002).
[8] J. C. Loudon and P. A. Midgley, Phys. Rev. Lett. **96**, 027214 (2006).
[9] E. Dagotto, Science **309**, 257 (2005).
[10] G. C. Milward *et al.*, Nature (London) **433**, 607 (2005).
[11] R. Akiyama *et al.*, Appl. Phys. Lett. **79**, 4378 (2001).
[12] K. Matsuba *et al.*, Physica (Amsterdam) **388C**, 281 (2003).
[13] K. McElroy *et al.*, Science **309**, 1048 (2005).
[14] S. J. L. Billinge *et al.*, Phys. Rev. Lett. **77**, 715 (1996).
[15] C. H. Booth *et al.*, Phys. Rev. Lett. **80**, 853 (1998).
[16] P. G. Radaelli *et al.*, Phys. Rev. B **54**, 8992 (1996).
[17] D. Louca *et al.*, Phys. Rev. B **56**, R8475 (1997).
[18] S. J. L. Billinge *et al.*, Phys. Rev. B **62**, 1203 (2000).
[19] T. Proffen and S. J. L. Billinge, Appl. Phys. A **74**, s1770 (2002).
[20] E. Dagotto *et al.*, Phys. Rep. **344**, 1 (2001).
[21] N. E. Massa *et al.*, J. Magn. Magn. Mater. **233**, 91 (2001).
[22] B. Dabrowski *et al.*, J. Solid State Chem. **146**, 448 (1999).
[23] P. F. Peterson *et al.*, J. Appl. Crystallogr. **36**, 53 (2003).
[24] P. F. Peterson *et al.*, J. Appl. Crystallogr. **33**, 1192 (2000).
[25] T. Proffen and S. J. L. Billinge, J. Appl. Crystallogr. **32**, 572 (1999).
[26] A. C. Larson and R. B. Von Dreele, Los Alamos Laboratory Report No. LAUR-86-748, 1987.
[27] T. Proffen *et al.*, Phys. Rev. B **60**, 9973 (1999).
[28] P. G. Radaelli *et al.*, Phys. Rev. B **55**, 3015 (1997).
[29] E. O. Wollan and W. C. Koehler, Phys. Rev. **100**, 545 (1955).
[30] X. Qiu *et al.*, Phys. Rev. Lett. **94**, 177203 (2005).
[31] J. Rodriguez-Carvajal *et al.*, Phys. Rev. B **57**, R3189 (1998).
[32] S. J. Hibble *et al.*, J. Phys. Condens. Matter **11**, 9221 (1999).
[33] R. Bindu *et al.*, J. Phys. Condens. Matter **17**, 6393 (2005).
[34] M. N. Iliev *et al.*, Phys. Rev. B **57**, 2872 (1998).
[35] L. Vegard, Z. Phys. **5**, 17 (1921).
[36] J. C. Mikkelson and J. B. Boyce, Phys. Rev. Lett. **49**, 1412 (1982).
[37] I.-K. Jeong *et al.*, Phys. Rev. B **63**, 205202 (2001).
[38] J. van Elp and A. Tanaka, Phys. Rev. B **60**, 5331 (1999).
[39] G. Zampieri *et al.*, Phys. Rev. B **58**, 3755 (1998).
[40] M. Pissas *et al.*, Phys. Rev. B **72**, 064425 (2005).